RESEARCH PAPER

Formulation and Evaluation of Nanosponges containing Antipsychotic Drugs for Brain Targeting via Nasal Route

Mr. Bhaskar P. Mhetre*[1], Dr. Nagesh Aloorkar[2]
[1,2]Satara College of Pharmacy, Degaon, New additional MIDC, Degaon, behind Spicer India, Ltd, Satara, Maharashtra 415004
***Corresponding author: Bhaskar P. Mhetre, Satara College of Pharmacy, Degaon, New additional MIDC, Degaon, behind Spicer India, Ltd, Satara, Maharashtra 415004**
Email: mhetrebhaskrar@gmail.com
Received: 28th May, 2026; **Revised:** 10th June, 2026; **Accepted:** 13th June, 2026; **Available Online:** 14th June, 2026

ABSTRACT

Background

This study aimed to develop a nanosponge-loaded intranasal in situ gel of Risperidone for improved brain targeting, enhanced bioavailability, and controlled drug release.

Materials and Methods

Risperidone nanosponges (RF1–RF13) were prepared using the quasi-emulsion solvent diffusion method and evaluated for drug content, entrapment efficiency, particle size, PDI, zeta potential, and in vitro release. The optimized nanosponge was incorporated into intranasal in situ gels (MR1–MR13) using poloxamer 407 and HPMC and assessed for physicochemical properties, mucoadhesion, drug content, and release kinetics. Pharmacokinetic studies were performed to determine absorption, distribution, and systemic persistence.

Results

RF1 showed the highest drug content (96.3%) and entrapment efficiency (94.23%) with particle size 152 nm, PDI 0.172, and zeta potential −29.1 mV, releasing 96.86% of drug at 60 min following zero-order kinetics ($R^2 = 0.9813$). Among in situ gels, MR5 was optimized with pH 6.2, gel strength 60.07 s, gelling time 12.35 s, viscosity 14,890 cps, mucoadhesive strength 1365 dynes/cm², spreadability 16.11 gm•cm/sec, and drug content 98.47%, showing 98.18% drug release at 60 min ($R^2 = 0.9983$). TEM confirmed spherical nanoparticles (50–145 nm), and stability studies showed minimal changes over 3 months (drug content 98.39%, release 98.09%). Pharmacokinetics revealed rapid absorption with Cmax of 4.29 µg/mL (IV) and 3.49 µg/mL (nasal) at 2 h (Tmax), no absorption lag (Tlag = 0), long half-life (t1/2 ≈ 39–41 h), and mean residence time (MRT ≈ 58–60 h). Low volume of distribution (Vss ≈ 0.12–0.14 L/kg) suggested drug remained largely in the vascular compartment, with limited sampling capturing <21% of total exposure, indicating extrapolated elimination.

Conclusion

The nanosponge-loaded intranasal in situ gel demonstrated excellent drug loading, stability, mucoadhesion, and controlled release. The optimized MR5 formulation combines favorable pharmacokinetics with effective brain targeting, offering a promising approach for enhanced CNS therapy and reduced systemic side effects.

Keywords: Risperidone, Nanosponges, Intranasal delivery, In situ gel, Brain targeting, Controlled release.
How to cite this article: Mhetre BP, Aloorkar N. Formulation and Evaluation of Nanosponges containing Antipsychotic Drugs for Brain Targeting via Nasal Route. Int J Drug Deliv Technol. 2026;16(60s):308-325. DOI: 10.25258/ijddt.16.60s.36
Source of support: Nil.
Conflict of interest: None

1. Introduction

Neurological and psychiatric disorders, including schizophrenia, bipolar disorder, and depression, pose a significant global health burden, with schizophrenia affecting millions worldwide. Conventional antipsychotic therapy, such as oral or parenteral Risperidone, is often limited by poor brain bioavailability due to the restrictive blood–brain barrier (BBB), extensive first-pass metabolism, and systemic side effects, including metabolic, cardiovascular, and extrapyramidal complications [1–4]. The BBB, composed of tightly connected endothelial cells and active efflux transporters such as P-glycoprotein, selectively permits small and lipophilic molecules while blocking most drugs, creating a major challenge for CNS therapy [5–7].

Intranasal (IN) drug delivery has emerged as a promising non-invasive approach to bypass the BBB via olfactory and trigeminal pathways. This route allows direct brain targeting, rapid onset of action, reduced systemic toxicity, and improved patient

compliance. Drugs administered intranasally can reach the brain through intraneuronal transport, involving vesicular movement along axons, or extraneuronal transport, including paracellular diffusion through tight junctions and transcellular pathways. While the olfactory region allows direct CNS access, the respiratory region contributes indirectly through systemic absorption. However, IN delivery faces limitations such as mucociliary clearance, enzymatic degradation, limited residence time, and small dosing volumes (0.2–0.4 mL), which make conventional Risperidone formulations difficult to administer effectively [8–10].

Nanosponges, three-dimensional, porous, cross-linked polymeric carriers, represent a promising strategy for enhancing the delivery of poorly soluble drugs like Risperidone via the nasal route. These structures can encapsulate both hydrophilic and lipophilic drugs, improve solubility, protect the drug from enzymatic degradation, provide sustained release, and enhance pharmacokinetics. When combined with intranasal delivery, nanosponges can prolong residence time in the nasal cavity, improve mucosal permeability, and enable efficient brain targeting with reduced dose and systemic toxicity [11–13].

To further improve nasal retention and drug absorption, nanosponge formulations can be incorporated into in situ gel systems, which undergo sol-to-gel transition upon contact with nasal physiological conditions such as temperature, pH, or ionic strength. These nanosponge-loaded in situ nasal gels offer additional advantages, including prolonged residence time at the site of administration, reduced mucociliary clearance, enhanced mucoadhesion, and controlled drug release. The gel matrix acts as a depot system, allowing sustained release of Risperidone-loaded nanosponges, thereby improving drug permeation through the nasal mucosa and enhancing brain targeting efficiency. Moreover, such systems provide ease of administration, improved stability, and better patient compliance, making them highly suitable for long-term management of CNS disorders.

The present research focuses on the formulation and evaluation of nanosponge-based Risperidone incorporated into an in situ nasal gel for brain targeting via the intranasal route, aiming to improve CNS drug accumulation, minimize systemic adverse effects, and achieve rapid as well as sustained therapeutic action. This approach highlights the potential of combining nanotechnology with intranasal in situ gel systems to overcome the limitations of conventional Risperidone therapy and enhance therapeutic outcomes in schizophrenia and related psychiatric disorders [14–16].

2. Materials and Methods

2.1 Materials

Risperidone was kindly gifted by Cipla Ltd., Vikhroli west, Mumbai, India**.** Ethyl cellulose (mg) and β-cyclodextrin (mg) were procured from Merck Life Science Pvt. Ltd., Mumbai, India. Polyvinyl alcohol (%) was obtained from Loba Chemie Pvt. Ltd., Mumbai, India. Poloxamer 407, HPMC and benzalkonium chloride were procured from Merck Life Science Pvt. Ltd., Mumbai, India. Methanol and ethanol were purchased from Merck Life Science Pvt. Ltd., Mumbai, India. All chemicals and reagents were of analytical grade and used as received.

2.2 Methods

2.2.1 Method of preparation of Risperidone Nanosponge

Nanosponge were prepared by quasi-emulsion solvent diffusion method using an external phase of distilled water and polyvinyl alcohol (PVA) and the internal phase consisted of the drug, β-cyclodextrin, and ethyl cellulose polymer dissolved in methanol, For preparing Nanosponge, the internal phase was prepared and added to the external phase at room temperature. Continuous stirring was maintained for 2 hours during the emulsification process. Then the Nanosponges were separated by filtration. The product was washed and dried by vacuum oven at 40°C for 12 hrs [17].

Table 1: DOE Suggested and experimental batches

Formulation code	Risperidone (mg)	Ethyl cellulose (mg)	Polyvinyl alcohol (%)	B-cyclodextrin (mg)	Stirring speed (rpm)	Methanol (ml)
RF1	10	450	0.75	20	1500	20
RF2	10	600	1	20	1500	20
RF3	10	600	0.75	20	2000	20
RF4	10	600	0.75	20	1000	20
RF5	10	450	0.5	20	1000	20
RF6	10	450	0.75	20	2000	20
RF7	10	600	0.5	20	1500	20
RF8	10	300	1	20	1500	20

RF9	10	300	0.5	20	1500	20
RF10	10	450	0.5	20	2000	20
RF11	10	300	0.75	20	2000	20
RF12	10	300	0.75	20	1000	20
RF13	10	450	1	20	2000	20

3. Evulation of Risperidone nanosponges

3.1 Drug content %)

The drug content in the Nanosponge was determined by dissolving 10 mg of Nanosponge in 10 ml of Methanol. Absorbance of the solution was then measured spectrophotometric ally at 277 nm after filtration and appropriate dilution with Methanol and drug content in the Nanosponge was determine. [18] Drug Content was calculated as follows:

$$Drug\ content\ (\%) = \frac{\text{Actual concentration of drug in the formulation}}{\text{Theoretical concentration of drug}} \times 100$$

3.2 Entrapment efficiency of Risperidone loaded nanosponge

Accurately weighed nanosponge (10 mg) was dispersed in 10 mL methanol and shaken at 37 ± 0.5 °C for 2 h. The dispersion was centrifuged at 15000 rpm for 30 min, and the supernatant was filtered (Whatman No. 40). Drug content was analyzed at 277 nm using a UV spectrophotometer, and % entrapment efficiency was calculated using the standard formula [19].

$$\text{Entrapment efficiency}(\%) = \frac{Added\ drug - Free\ drug}{Added} \times 100$$

3.3 Particle Size, PDI and Zeta potential (HORIBA SZ-100)

The 10 mg Nanosponge formulation was taken and mixed with distilled water and sonication was kept for 30 min. The analysis was performed at a temperature of 25 ℃. Same procedure repeated at zeta potential. [20]

3.4 In vitro Dissolution study

In vitro studies were carried out using a USP type II dissolution apparatus. The nanosponge powder was placed in 900ml of Phosphate buffer ph 6.4 at paddle speed of 50 rpm maintained at 37°C ± 0.5°C for 2 hrs. 5 ml of Sample was taken at specific time intervals 10, 20,30,40,50 and 60 min analyzed using UV spectrophotometer (Jasco v-630) at 277 nm. [21]

3.5 FTIR spectroscopy

The drug excipients compatibility study was performed by FTIR technique. The Optimized batches RF1 samples were scanned over wave number range of 500-4000 cm-1 with diffraction reflectance scanning technique [22].

3.6 Differential Scanning Calorimetry (DSC)

Differential scanning calorimetric (DSC) measurements were carried out on a modulated DSC (Mettler Toledo, SW STARe, and USA). The Optimized batch RF1 were weighed (2-8mg), the aluminum pans were used and hermetically covered with lead. The heating rage was 50-250 °C for sample with constant increasing rate of temperature at 10°C /min under nitrogen atmosphere (50-60ml/min). The resultant thermograms of formulation was obtained. [23]

3.7 Scanning Electron microscopy

Scanning Electron microscopy **(**SEM) (Carl Zeiss, supra55, Germany) at the central instrumental facility (YCIS SATARA). Photographs of samples were taken by a different magnification power (200 x 500x).electron microscopy is used to determine the morphology of fractured, surface topography, and texture. The surface morphology of optimized batches was determined. [24]

3.8 X-ray Diffraction Study

The data obtained from XRD was used to determine whether newly formed compounds are crystalline or amorphous, the following conditions were used for the measurement: target metals Cu, filter K, 40kV voltage, and 30 mA current. Optimized batch RF1 Samples were scanned over a two-degree range of 10–90°C with a 0.2° phase scale. [25]

2.3 Drug containing nanosponge loaded nasal in setu gel

In situ gels were prepared using the cold method. A calculated amount of a mucoadhesive polymer (HPMC K4M) and Drug loaded nanosponges (mg) was dissolved in water. Poloxamer 407 was added slowly to the water with continuous stirring on a magnetic stirrer. The dispersion was then stored in a refrigerator until clear solution is obtained. [26, 27]

Table 2: Experimental batches suggested by DOE

Formulation	Drug load	concentration	concentration	stirring	Benzalkonium	Distilled

n code	ed nano spon ges (mg)	of Polo xame r (% w/v)	of HP MC	sp eed	chlor ide (%)	wa ter (q. s)
MR1	480	17	0.8	10 00	0.01	10 0
MR2	480	18	0.6	10 00	0.01	10 0
MR3	480	16	0.6	15 00	0.01	10 0
MR4	480	17	0.4	10 00	0.01	10 0
MR5	480	18	0.8	12 50	0.01	10 0
MR6	480	17	0.6	12 50	0.01	10 0
MR7	480	16	0.8	12 50	0.01	10 0
MR8	480	17	0.4	15 00	0.01	10 0
MR9	480	18	0.6	15 00	0.01	10 0
MR1 0	480	18	0.4	12 50	0.01	10 0
MR1 1	480	17	0.8	15 00	0.01	10 0
MR1 2	480	16	0.6	10 00	0.01	10 0
MR1 3	480	16	0.4	12 50	0.01	10 0

4. Evaluation of drug containing nanosponge loaded nasal in situ gel

4.1 Physical appearance

4.2 Determination of pH

One ml of the prepared gels was transferred to a 10 ml volumetric flask, and the solution was diluted with distilled water. The pH of resulting solution is determined using a digital pH meter (Contech), which was previously calibrated using phosphate buffers at pH 4 and pH 7.[28]

4.3 Gel strength

Sample (50 g) was placed in a 100 ml graduated cylinder. Gelation was carried out by placing the formulations in a thermostat at 37 °C. The strength of the gel was determined by measuring the time taken by a weight of 35 g to sink 5 cm in the gel.[29]

4.4 Gelling time

Gelling time was measured as the onset of gelation. For $T_{sol-gel}$, 2 mL of formulation was placed in a 10 mL test tube, equilibrated at each temperature in a 37 °C water bath for 10 min, and observed horizontally for gel formation. [30].

4.5 Viscosity

Viscosity of gel is determined using Brookfield viscometer (S-62, model LVDV-E) at 25 o C with a spindle speed of the viscometer rotated at 12 rpm.[31]

4.6 Mucoadhesive strength

Mucoadhesive force, the detachment stress of the formulation from nasal mucosa, was measured using a modified balance with sheep nasal mucosa (0.6 mm thick, 2.835 cm^2). Gel (0.5 mL) was placed between mucosal membranes, and the minimum weight of water needed to break adhesion was recorded. Mucoadhesive strength (dynes/cm^2) was calculated as:

Mucoadhesive Strength (dynes/cm^2) = mg/A

where m is weight for detachment (g), g = 980 cm/s^2, and A is mucosal surface area (cm^2).

4.7 Spreadability

For the determination of Spreadability excess of sample was applied in between two glass slides and was compressed to uniform thickness by placing 1000g weight for 5 min. Weight (50 g) was added to the pan. The time in which the upper glass slide moves over to the lower plate is taken as measure of Spreadability. [32]

S=ML/T

Where, M= weight tide to upper slide, L= length moved on the glass slide, T= time taken.

4.8 Drug content

1ml of formulation was taken in 10ml volumetric flask, diluted using distilled water adjust to 10ml. 1ml quantity from this solution was again diluted with 10ml of distilled water. Finally, the absorbance of prepared solution was measured at 277 nm against blank reagent using UV visible spectrophotometer (JASCO V-630). The concentration of the drug present in formulation was computed from the calibration curve using the equation: [33]

4.9 Ex-vivo drug permeation study

For in vitro diffusion study: Nasal mucosa and Franz diffusion cell was used for permeation study. Nasal mucosa was placed in between the donor and the receptor compartment. Gel containing drug was applied on surface of Nasal mucosa. It was in contact with receptor compartment containing 25mL of phosphate buffer pH 6.4. The cell was agitated by a magnetic stirrer at 50 rpm and maintained at 37°C. Aliquots withdrawn at intervals till 6 hr and replaced with equal volume of fresh phosphate buffer pH 6.4.

Absorbance was measured at 277 nm using UV visible spectrophotometer (JASCO V-630) [34].

4.10 Transmission Electron Microscopy (TEM) (JEOL, 2200FS)

The surface morphology of the optimized batch MR5 was examined using Transmission Electron Microscopy (TEM). A few microliters of diluted in situ nasal gel were placed on a 300-mesh copper grid, air-dried, and stained with 2% phosphotungstic acid. Excess stain was removed, and images were captured using digital micrograph and Soft Imaging Viewer software [35].

4.11 Stability study

According to ICH stability guidelines, the stability study was performed to assess the physical stability of the formulations. The study was conducted for a period of 3 months under long-term storage conditions of 25 ± 2 °C and 60 ± 5% relative humidity, as recommended by ICH. The formulations were evaluated at 30-day intervals, and at the end of 90 days they were assessed for pH, viscosity, and drug content to ensure stability and compliance with ICH requirements. [36]

4.12 Pharmacokinetic study of Resperidone in rabbit plasma as per the ICH Guidelines

Blood samples were collected from rabbits (n = 1 per group) following intravenous (3 mg/kg) and nasal (0.09 mg/kg) administration of Resperidone. At pre-dose and 0.05, 1, 2, 4, 6, 8, and 12 h post-dose, 100 µL of blood was drawn into Na_2EDTA tubes, vortexed for 10 min, and centrifuged at 4500 rpm at 20°C. The plasma supernatant was transferred to labelled tubes, evaporated at 40°C to dryness, reconstituted with 500 µL acetonitrile, vortexed briefly, and transferred to vials for injection.

- **Linearity**

Standard solutions of Resperidone were prepared, and the total area under the curve (AUC) versus time was calculated using the linear trapezoidal rule. The data were then used to determine the regression equation and correlation coefficient (R^2).

- **PK data analysis**

PkSolver Version2.0 pharmacokinetic software was used to analyze the plasma concentration of Nasal and IV administration of Resperidone API and Formulation using a noncompartmental model following oral administration in rat.

Plasma concentration *vs.* time data of Nasal and IV administration of Resperidone API and Formulation was analysed by Pk solver version 2.0 to derive various pharmacokinetic parameters, *viz.*, $AUC_{0\text{-}t}$, $AUC_{0\text{-}\infty}$, C_{max}, t_{max} and $t½$.

5. Results and Discussion

5.1 Drug content (%) and Entrapment efficiency (%)

Table 3: Drug Content and Entrapment efficiency RF1- RF13

Formulation code	Drug Content (%)	Entrapment efficiency (%)
RF1	96.3±0.0008	94.23±0.001
RF2	84.9±0.0006	80.14±0.003
RF3	87.6±0.0003	84.57±0.015
RF4	84.6±0.0005	80.14±0.006
RF5	86.8±0.0004	83.47±0.008
RF6	88.8±0.0009	85.29±0.014
RF7	89.6±0.0008	86.78±0.096
RF8	70.1±0.0006	61.21±0.025
RF9	92.5±0.0016	89.42±0.015
RF10	69.1±0.0013	64.55±0.069
RF11	85.1±0.0017	82.17±0.004
RF12	72.7±0.0003	65.45±0.098
RF13	83.6±0.0005	80.25±0.008

Conclusion

Drug content and entrapment efficiency of RF1–RF13 showed a similar trend, ranging from 69.1–96.3% and 61.21–94.23%, respectively. RF1 exhibited the highest values for both parameters, indicating efficient drug loading and uniformity, while RF8, RF10, and RF12 showed comparatively lower values. Overall, RF1 was identified as the optimized formulation.

ANOVA for Quadratic model

Response 1: Drug content

Drug Content =92.55+3.29A−6.44B+4.18C+4.43AB−2.35AC+13.36BC+1.19A2−9.47B2−11.24C2

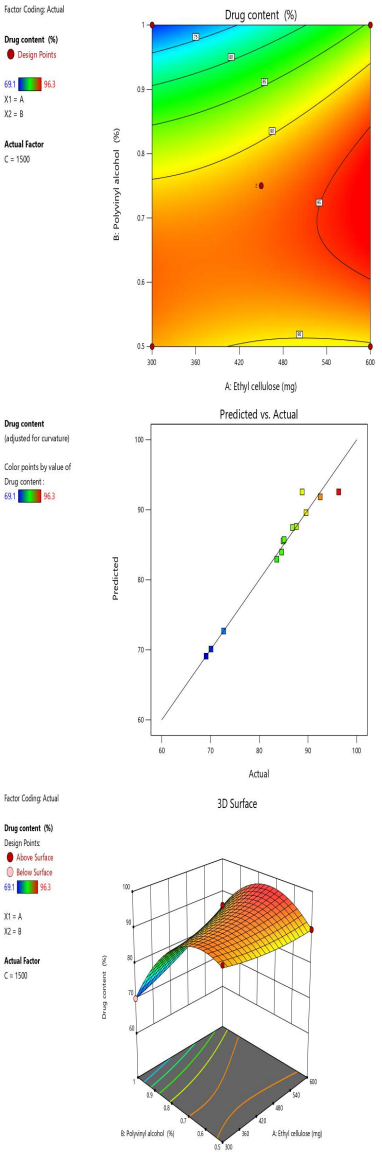

A) B)
C)

Figure 1A: Counter plot, Figure 2B: Predicted vs Actual plot, Figure 3C: 3D Surface plot

ANOVA for Quadratic model

Response 2: Entrapment efficiency

Entrapment Efficiency=89.76+4.17A−8.26B+5.74C+5.39AB−3.07AC+15.66BC+0.7525A2−11.12B2−12.4

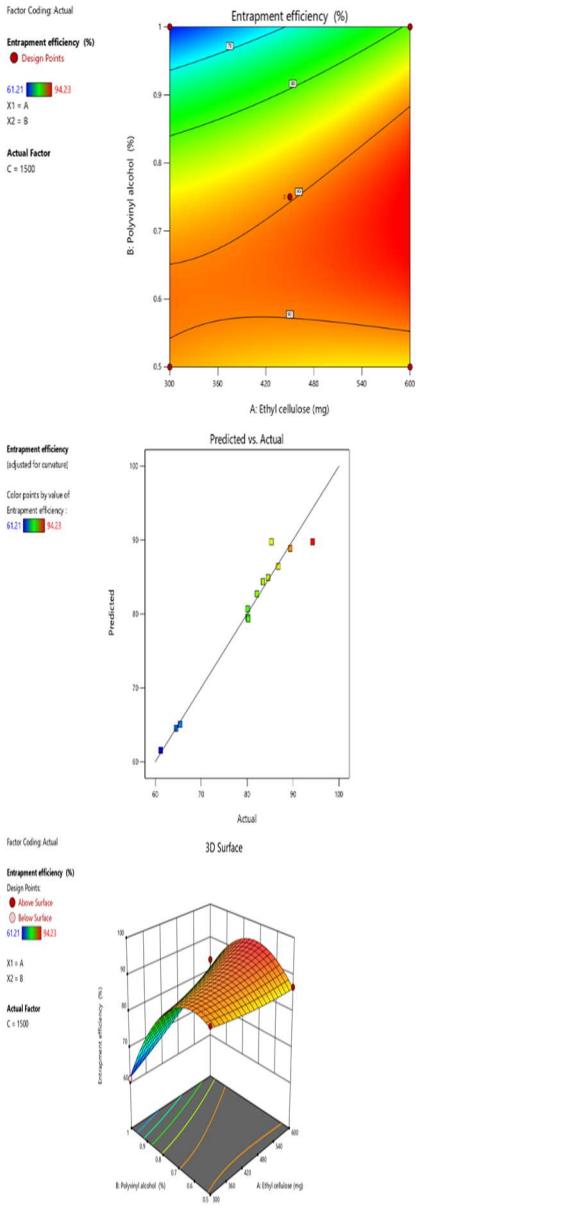

A) B)
C)

Figure 4A: Counter plot, Figure 5B: Predicted vs Actual plot, Figure 6C : 3D Surface plot

5.2 Particle Size, PDI and Zeta potential (HORIBA SZ-100)

Table 4: Particle Size, PDI and Zeta potential of RF1-RF13

Formulation code	Particle size (nm)	PDI	Zeta potential (mV)
RF1	152.0	0.172	-29.1

RF2	167.0	0.308	-25.6
RF3	175.2	0.338	-24.3
RF4	193.1	0.364	-24.8
RF5	179.5	0.292	-26.1
RF6	184.5	0.419	-23.5
RF7	170.8	0.332	-26.7
RF8	195.2	0.405	-25.3
RF9	179.3	0.322	-22.9
RF10	181.0	0.407	-28.3
RF11	186.0	0.341	-27.8
RF12	187.5	0.373	-20.6
RF13	169.6	0.372	-19.4

Conclusion

The particle size of formulations RF1–RF13 ranged from 152.0 to 195.2 nm, with RF1 showing the smallest size. PDI values indicated moderate to good uniformity, with RF1 exhibiting the lowest PDI (0.172), suggesting better homogeneity. Zeta potential values ranged from −19.4 to −29.1 mV, indicating good stability of the formulations. Overall, RF1 was identified as the optimized formulation due to its smaller particle size, low PDI, and high stability.

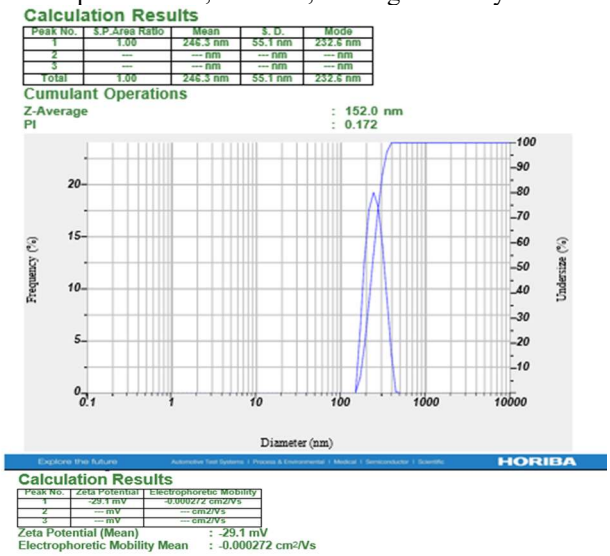

Figure 7: Particle size and PDI of RF1

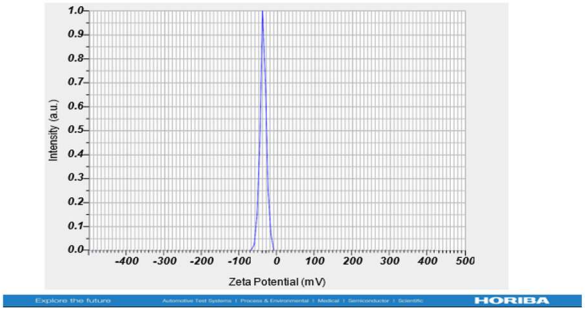

Figure 8: Zeta potential of RF1

5.3 In vitro Dissolution study

Table 5: Drug Release Study of RF1-RF7

Time (Min)	RF1	RF2	RF3	RF4	RF5	RF6	RF7
0	**0**	**0**	**0**	**0**	**0**	**0**	**0**
10	19.83±0.0038	11.54±0.0002	18.54±0.0002	17.01±0.0002	11.80±0.00025	13.67±0.00020	9.18±0.00015
20	25.18±0.003	19.43±0.0017	34.79±0.001	21.01±0.0015	19.23±0.0015	18.29±0.015	17.43±0.002
30	43.74±0.002	37.80±0.001	56.39±0.0015	37.50±0.001	21.27±0.015	29.35±0.035	38.12±0.0025
40	70.66±0.001	57.22±0.002	68.18±0.0015	54.34±0.003	49.34±0.051	51.84±0.015	51.42±0.043
50	87.36±0.0025	81.01±0.002	82.02±0.004	78.50±0.015	65.96±0.01	78.93±0.015	72.02±0.004
60	96.86±0.0025	94.02±0.002	92.76±0.004	80.92±0.015	83.72±0.015	89.67±0.03	81.05±0.015

Table 6: Drug Release Study of RF8-RF13

Time (Min)	RF8	RF9	RF10	RF11	RF12	RF13
0	**0**	**0**	**0**	**0**	**0**	**0**
10	16.83±0.0003	18.58±0.002	9.18±0.0025	8.70±0.020	16.63±0.0002	16.35±0.00035
20	19.14±0.003	29.42±0.0003	17.08±0.00015	16.08±0.0025	19.06±0.00023	26.73±0.00025

30	29.56±0.001	41.60±0.0025	27.45±0.00025	39.68±0.00025	29.75±0.0001	45.68±0.0002
40	57.22±0.0045	70.52±0.00153	58.14±0.002	59.87±0.0001	47.76±0.0004	63.75±0.0025
50	72.54±0.0015	86.17±0.0003	70.87±0.00025	78.24±0.00015	74.68±0.003	80.13±0.0035
60	88.62±0.00025	92.45±0.0001	88.67±0.0003	92.83±0.0004	89.59±0.0001	95.21±0.0002

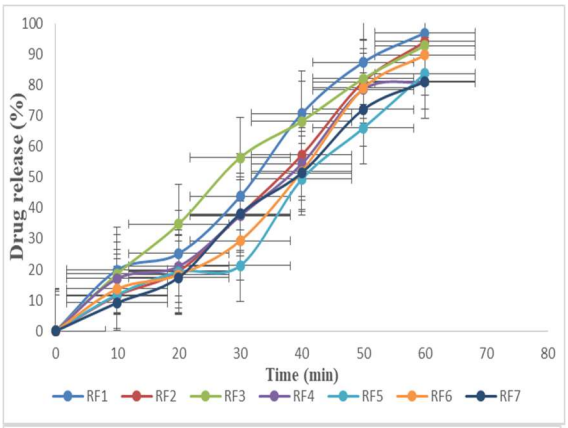

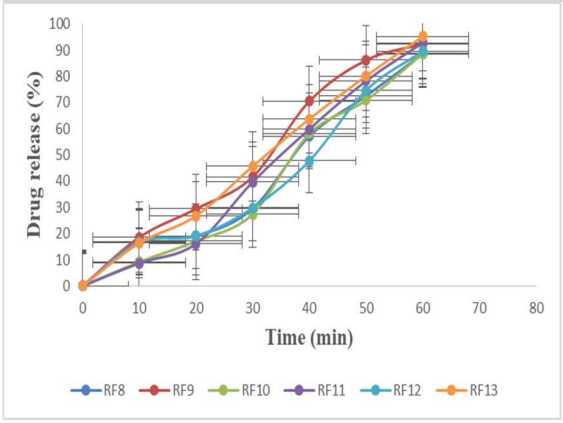

Figure 9: Drug Release Study of RF1-RF7 Figure 10: Drug Release Study of RF8-RF13

Conclusion

All formulations exhibited a time-dependent increase in drug release. RF1 showed the highest and fastest release (96.86% at 60 min), followed closely by RF13 and RF2, indicating efficient drug diffusion. In contrast, RF8 and RF10 showed comparatively slower release profiles. Overall, RF1 demonstrated superior drug release behavior and was considered the optimized formulation.

ANOVA for 2FI model

Response 3: Drug release

Drug release (%)=89.62−1.84A+2.53B+3.37C+4.20AB+2.15AC+0.4895BC

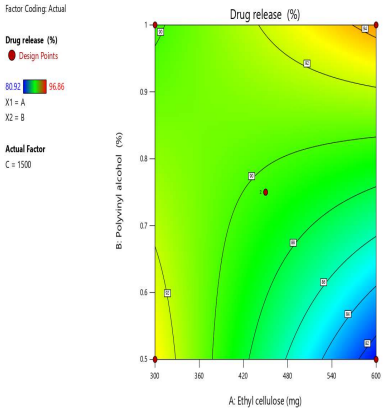

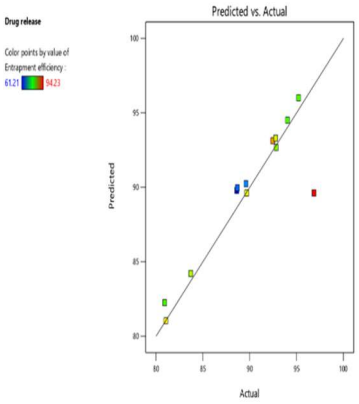

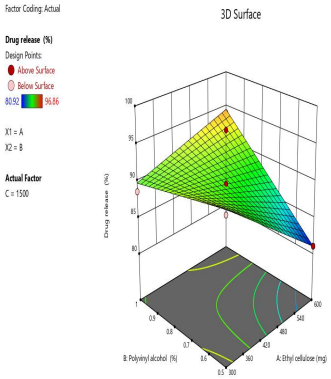

A) B) C)

Figure 11A: Counter plot, Figure 12B: Predicted vs Actual plot, Figure 13C : 3D Surface plot

Kinetic analysis of drug release

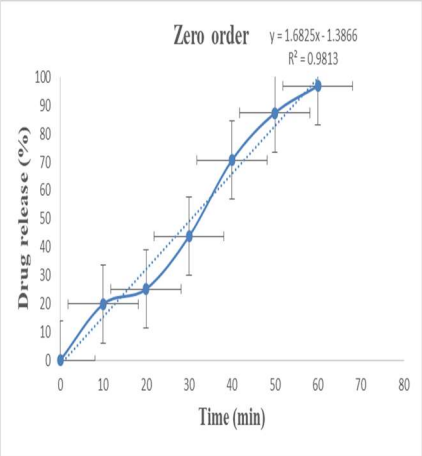

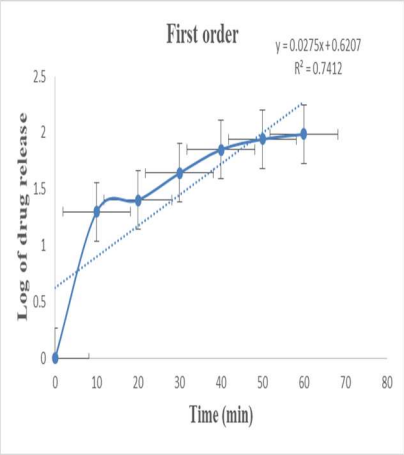

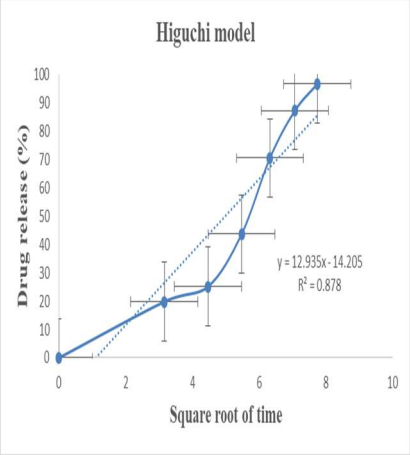

A) **B)**

C)

Figure 14A: First order, Figure 15B: Second order, Figure 16C: Third order

Conclusion

The in vitro release data of RF1 best fit the zero-order model (R^2 = 0.9813), indicating a constant and controlled drug release over time. Lower R^2 values for first-order (0.7412) and Higuchi (0.878) models suggest that release was independent of drug concentration and diffusion-controlled mechanisms were less dominant.

5.4 FTIR spectroscopy

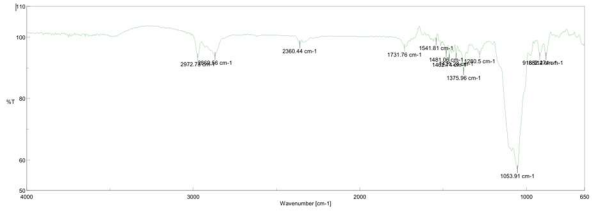

Figure 17: FTIR Spectrum of RF1

Conclusion

The FTIR spectrum of RF1 showed characteristic peaks for key functional groups: C=O stretching (1731.76 cm^{-1}), aliphatic C–H (2972.78 cm^{-1}), N–H bending (1541.81 cm^{-1}), aromatic C=C (1481.08–1429.05 cm^{-1}), methyl C–H (1375.96 cm^{-1}), C–O stretching (1053.91 cm^{-1}), and aromatic C–H bending (918.82 & 872.17 cm^{-1}). These results confirm the presence of ester, aromatic, and amide groups, indicating successful formation of the RF1 formulation.

5.5 Differential Scanning Calorimetry (DSC)

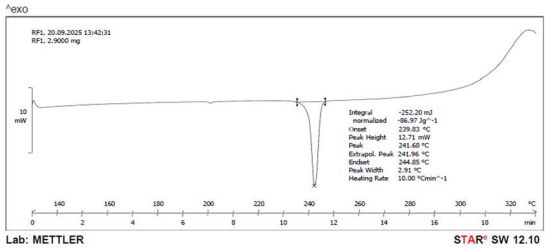

Figure 18: DSC thermogram of RF1

Conclusion

DSC of pure Risperidone showed a sharp peak at 172–173°C (crystalline). RF1 displayed a peak at ~241°C with no new transitions, indicating thermal stability. Peak shifts with Ethyl Cellulose suggest partial amorphization, confirming drug–excipient compatibility and a stable formulation.

5.6

5.7 Scanning Electron microscopy

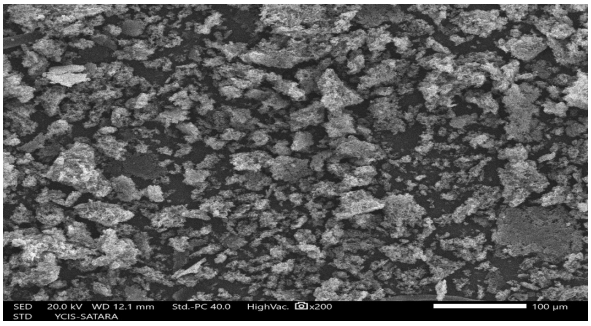

Figure 19: SEM of RF1

Conclusion –
The SEM image of RF1 nanosponges shows a porous, sponge-like structure with irregular morphology and rough surfaces, confirming nanosponge formation.

5.8 X-ray Diffraction Study

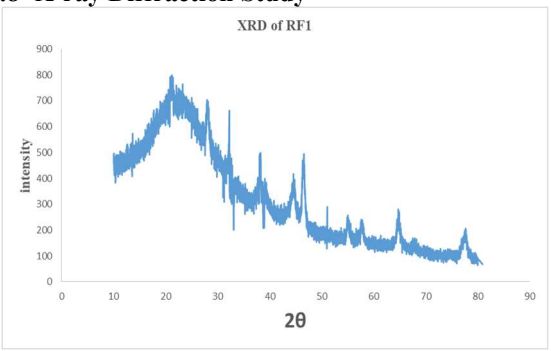

Figure 20: X-ray Diffractogram of RF1

Conclusion
The X-ray Diffractogram of RF1 shows a broad halo peak without any sharp or intense crystalline reflections, which is a clear indication of its amorphous nature. The absence of distinct crystalline peaks suggests that the drug has been successfully converted from its crystalline form into an amorphous form during the formulation process.

6. Results and Discussion of drug containing nanosponge loaded nasal in situ gel

6.1 Physical appearance, pH, Gel Strength, Gelling Time

Table 7: Physical appearance, pH, Gel Strength, Gelling Time

Formulation Code	Appearance	pH	Gel Strength (s)	Gelling Time (s)
MR1	Transparent	4.5	57.16 ± 0.12	11.17 ± 0.4
MR2	Transparent	5.7	51.08 ± 0.18	10.55 ± 0.2
MR3	Transparent	5.6	47.58 ± 0.61	4.56 ± 0.3
MR4	Transparent	4.7	49.33 ± 0.52	8.23 ± 0.4
MR5	Transparent	6.2	60.07 ± 0.44	12.35 ± 0.7
MR6	Transparent	6.8	48.34 ± 0.87	9.31 ± 0.6
MR7	Transparent	4.9	56.34 ± 0.63	9.34 ± 0.8
MR8	Transparent	5.1	50.39 ± 0.72	8.81 ± 0.4
MR9	Transparent	6.4	42.38 ± 0.94	7.18 ± 0.9
MR10	Transparent	5.8	50.29 ± 0.78	9.22 ± 0.4
MR11	Transparent	5.5	46.92 ± 0.37	10.19 ± 0.3
MR12	Transparent	5.4	53.88 ± 0.25	8.99 ± 0.8
MR13	Transparent	4.9	57.11 ± 0.19	9.64 ± 0.32

Conclusion
All formulations were transparent with pH ranging from 4.5 to 6.8, suitable for nasal administration. Gel strength varied between 42.38 and 60.07 s, with MR5 showing the highest strength, indicating better gel integrity. Gelling time ranged from 4.56 to 12.35 s, where MR3 showed the fastest gelation. Overall, MR5 demonstrated optimal properties with suitable pH, highest gel strength, and acceptable gelling time, making it the optimized formulation.

ANOVA for Quadratic model

Response 1: pH

pH=6.80+0.4125A+0.0750B+0.2875C+0.1000AB+0.1250AC+0.1500BC−0.2625A2−1.09B2−0.7625C2

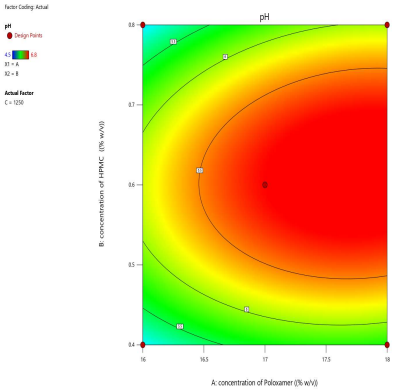

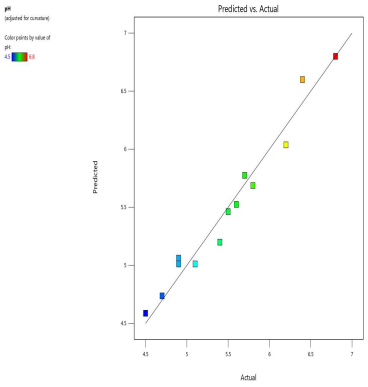

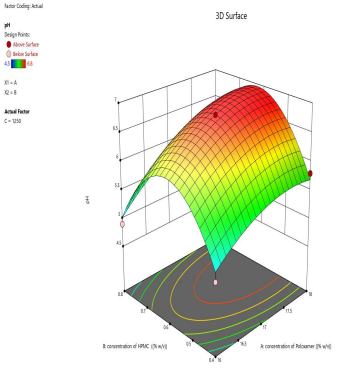

A) **B)**
C)

Figure 21A: Counter plot, Figure 22B: Predicted vs Actual plot, Figure 23C : 3D Surface plot

6.2 Viscosity

Table 8: Viscosity, Mucoadhesive Strength, Spreadability, Drug Content of MR1- MR13

Formulation Code	Viscosity (cps)	Mucoadhesive Strength (dynes/cm²) ± SD	Spreadability (gm·cm/sec) SD(±)	Drug Content (%)
MR1	9150	1185 ± 0.22	9.25	92.45 ± 0.23
MR2	8210	1210 ± 0.18	12.88	90.12 ± 0.18
MR3	14840	1135 ± 0.26	13.14	88.56 ± 0.21
MR4	10125	1258 ± 0.35	11.33	91.88 ± 0.19
MR5	14890	1365 ± 0.28	16.11	98.47 ± 0.25
MR6	13230	1280 ± 0.31	12.66	94.68 ± 0.22
MR7	13945	1235 ± 0.33	10.69	89.35 ± 0.20
MR8	13680	1198 ± 0.29	8.14	93.22 ± 0.24
MR9	13420	1174 ± 0.25	11.25	95.18 ± 0.21
MR10	13265	1205 ± 0.21	9.55	90.89 ± 0.23
MR11	13085	1156 ± 0.27	11.09	87.75 ± 0.18
MR12	12870	1182 ± 0.19	12.88	82.95 ± 0.22
MR13	12550	1216 ± 0.23	14.25	81.67 ± 0.20

Conclusion

All formulations exhibited acceptable viscosity, mucoadhesive strength, spreadability, and drug content, indicating suitability for nasal delivery. Among them, MR5 showed the highest viscosity (14890 cps), maximum mucoadhesive strength (1365 dynes/cm²), highest spreadability (16.11 gm·cm/sec), and maximum drug content (98.47%), suggesting superior formulation characteristics. Overall, MR5 was identified as the optimized in situ gel formulation with enhanced nasal retention, drug loading, and performance for effective brain targeting.

ANOVA for Linear model

Response 2: Viscosity

Viscosity=12558.46−552.50A+181.25B+1833.75C

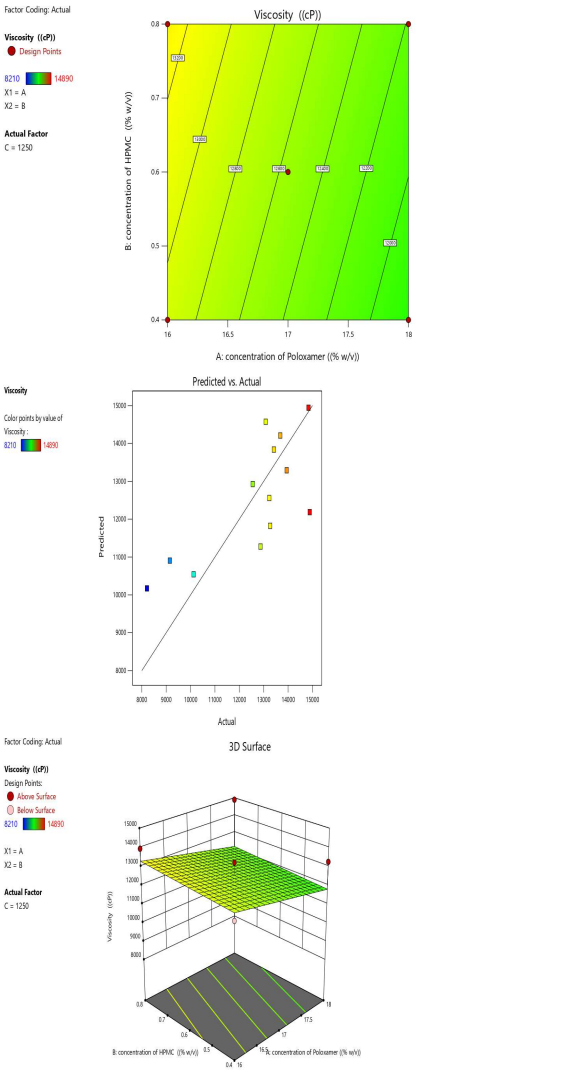

A) **B)**
C)

Figure 24A: Counter plot, Figure 25B: Predicted vs Actual plot, Figure 26C : 3D Surface plot

ANOVA for Linear model

Response 3: Drug Content

Drug Content=90.55+4.02A+1.29B+0.9138C

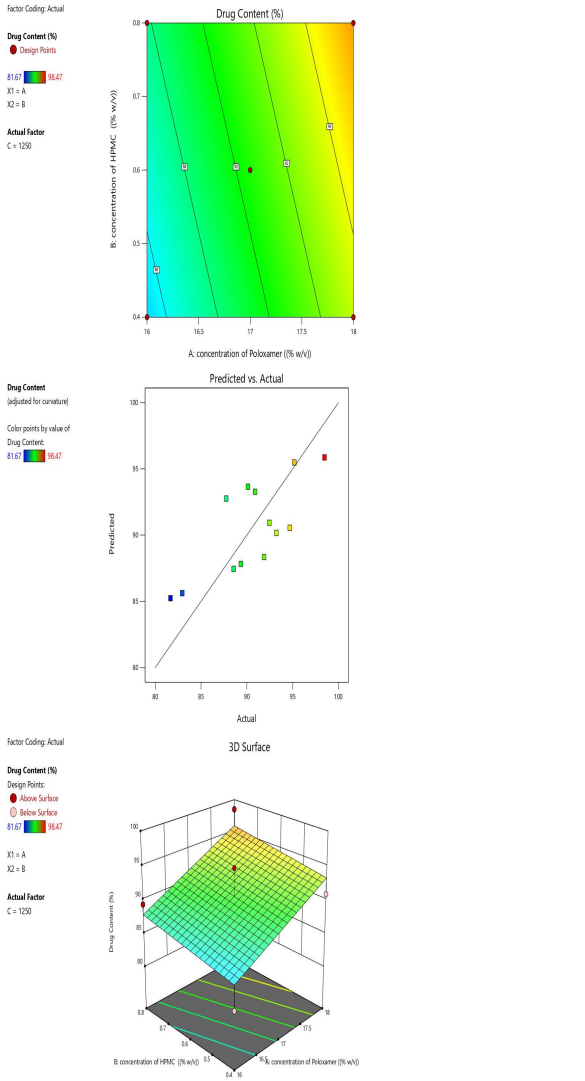

A) **B)**
C)

Figure 27A: Counter plot, Figure 28B: Predicted vs Actual plot, Figure 29C : 3D Surface plot

6.3 In Vitro Drug Release Study

Table 9: Drug release of MR1- MR7

Time (min)	MR1	MR2	MR3	MR4	MR5	MR6	MR7
0	0	0	0	0	0	0	0
10	13.91±0.012	7.66±0.614	14.37±0.378	14.40±0.001	13.41±0.96	13.41±0.05	17.55±0.006
20	34.58±	25.52±	26.08±	29.75±	33.01±	20.22±	34.96±

	0.025	0.035	0.006	0.429	0.047	0.017	0.248
30	49.66±0.009	33.22±0.0217	44.13±0.019	41.70±0.285	47.31±0.003	29.42±0.063	48.51±0.002
40	68.68±0.124	48.46±0.096	60.39±0.022	50.31±0.009	67.22±0.024	44.27±0.001	55.76±0.083
50	80.76±0.654	65.24±0.089	77.99±0.749	66.21±0.002	83.41±0.892	68.43±0.082	63.15±0.049
60	95.27±0.001	91.64±0.005	87.85±0.005	91.19±0.019	98.18±0.001	91.32±0.098	90.67±0.057

Table 10: Drug release of MR8- MR13

Time (min)	MR 8	MR 9	MR 10	MR 11	MR 12	MR 13
0	0	0	0	0	0	0
10	12.56±0.042	15.59±0.006	16.13±0.004	22.22±0.283	18.56±0.064	19.26±0.049
20	25.80±0.039	37.69±0.028	28.92±0.825	30.91±0.004	37.35±0.581	42.89±0.005
30	35.92±0.078	52.67±0.013	41.69±0.0372	46.27±0.069	51.56±0.824	59.77±0.096
40	41.49±0.009	63.85±0.095	52.24±0.0914	63.33±0.007	64.60±0.002	79.65±0.028
50	59.47±0.052	76.10±0.027	70.52±0.863	80.24±0.026	83.39±0.049	88.08±0.001
60	93.18±0.002	91.08±0.036	91.31±0.007	94.75±0.0012	93.77±0.037	96.98±0.057

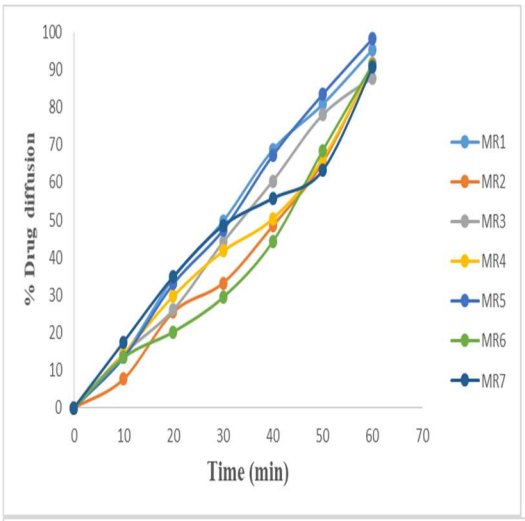

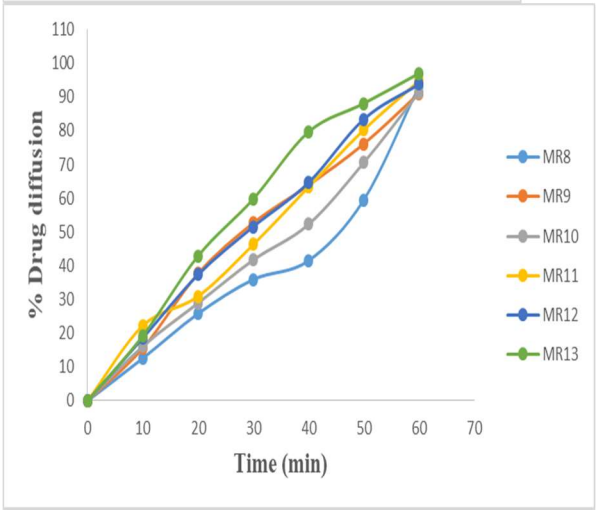

Figure 30: Drug release of MR1- MR1 Figure 31: Drug release of MR8- MR13

Conclusion

All formulations (MR1–MR13) exhibited a gradual and sustained drug release pattern over 60 minutes. Among them, MR5 showed the highest drug release (98.18%), indicating superior release characteristics and effective formulation performance. Most formulations achieved more than 90% drug release at 60 minutes, confirming efficient drug diffusion and suitability for intranasal delivery. Overall, MR5 was identified as the optimized formulation with maximum and controlled drug release.

Kinetic analysis of drug release

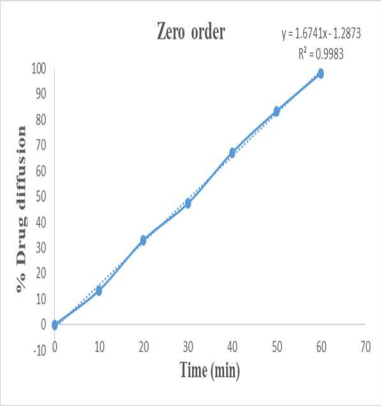

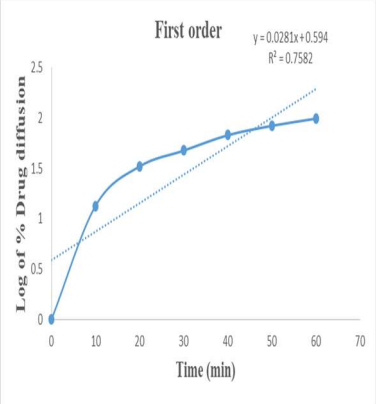

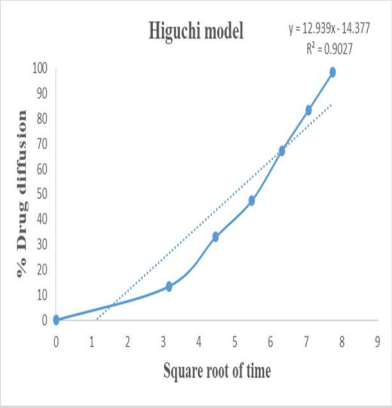

Figure 32: Zero order Figure 33: First order Figure 34: Higuchi model

Conclusion

The drug release from formulation MR5 followed zero-order kinetics ($R^2 = 0.9983$), indicating a constant and controlled release profile, with diffusion also contributing as per the Higuchi model.

6.4 Transmission Electron Microscopy (TEM) (JEOL, 2200FS)

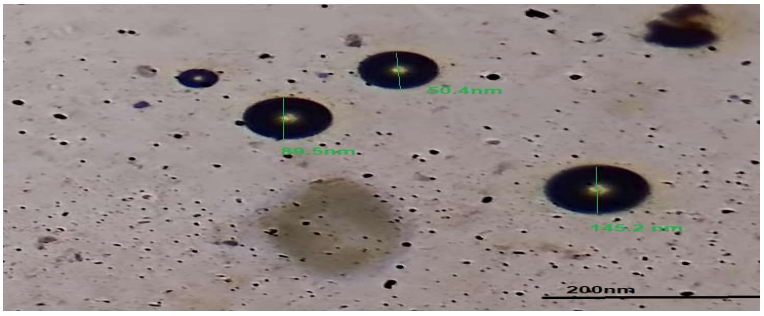

Figure 35: TEM of optimized batch (MR5)

Conclusion

The TEM analysis of optimized batch MR5 showed well-defined, spherical nanoparticles with smooth morphology and uniform distribution. Particle sizes ranged from ~50.4 to 145.2 nm, confirming nanoscale formation. The absence of aggregation indicated good stability and proper dispersion, validating the effectiveness of the formulation.

6.5 Stability study

Table 11: Stability study of optimized batch MR5

Parameter	Initial	1	2	3
Viscosity (%)	14890	14888	14884	14881
Drug content (%)	98.47 ± 0.25	98.45 ± 0.004	98.41 ± 0.081	98.39 ± 0.65
Drug release (%)	98.18± 0.001	98.15± 0.012	98.12± 0.025	98.09± 0.009

Conclusion:

The stability study of optimized batch MR5 showed negligible changes in viscosity (14890 to 14881 cps), drug content (98.47% to 98.39%), and drug release (98.18% to 98.09%) over 3 months, indicating good stability and consistency of the formulation under storage conditions.

6.6 Pharmacokinetic study of Resperidone in rabbit plasma as per the ICH Guidelines

- **Linearity**

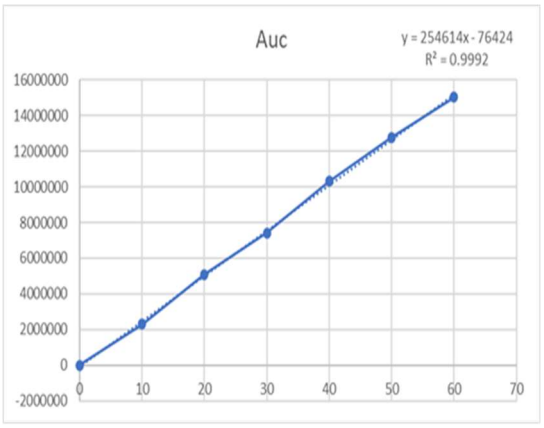

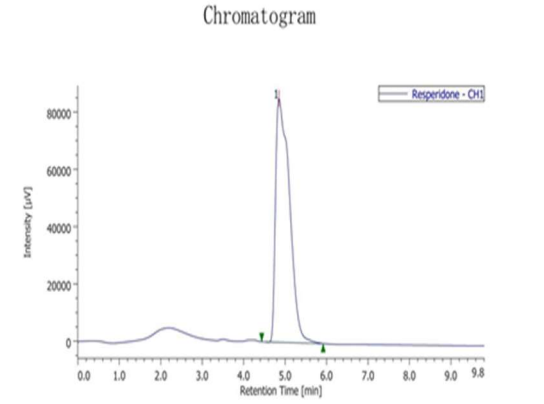

(a) **(b)**

Figure 36: Linearity graph of Resperidone (b), Figure 37: HPLC chromatogram – Linearity

- **PK data analysis**

Table 12: Summary Table- Input Variable- Resperidone Nasal

TIME IN Hrs	AUC	Conc.	Plasma Drug Conc.
0	7239	261853	3.426318957
0.5	9176	263790	3.451664399
1	6909	261523	3.422000942
2	4556	259170	3.391212185
4	3827	258441	3.381673296
6	5655	260269	3.405592484
8	7516	262130	3.429943473
12	12098	266712	3.489898461

Table 13: Summary Table- Output (Resperidone Nasal)

Time	Conc	ln(C)	AUC	AUMC
0	3.426319	1.2314865	0	0
0.5	3.4516644	1.2388565	1.7194958	0.431458
1	3.4220009	1.2302255	3.4379122	1.7184163
2	3.3912122	1.2211874	6.8445187	6.820629
4	3.3816733	1.2183706	13.617404	27.129747
6	3.4055925	1.2254189	20.40467	61.089995
8	3.4299435	1.2325438	27.240206	108.9631
12	3.4898985	1.2498726	41.07989	247.59976

Table 14: Calculation Results (Resperidone Nasal)

Parameter	Unit	Value
t1/2	h	39.1454111
Tmax	h	2
Cmax	µg/ml	3.489898461
Tlag	h	0
Clast_obs/Cmax		1
AUC 0-t	µg/ml*h	41.07988983
MRT 0-inf_obs	h	58.5478545

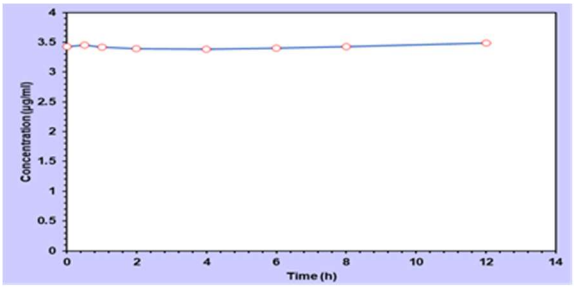

Figure 38: Time in (min) Vs Concentration (µg/ml) [Resperidone Nasal]

Conclusion

Non-compartmental analysis showed that Resperidone reached a peak concentration (Cmax) of 3.49 µg/mL at 2 h (Tmax), with no absorption lag (Tlag = 0). The drug exhibited a long half-life (t1/2 ≈ 39.15 h) and a mean residence time (MRT0–inf) of 58.55 h. Limited sampling near Tmax resulted in a relatively low AUC0–t (41.08 µg·h/mL), indicating that the elimination phase was not fully captured.

Table 15: Summary Table- Input Variable- Resperidone IV

TIME IN Hrs	AUC	Conc.	Plasma Drug Conc.
0	12967	267581	3.501269235
0.5	21676	276290	3.615225584
1	23207	277821	3.635258558
2	72919	327533	4.285734848
4	5669	260283	3.405775673
6	6990	261604	3.423060819
8	2324	256938	3.362006699
12	7496	262110	3.429681775

Table 16: Summary Table- Output (Resperidone IV)

Time	Conc	ln(C)	AUC	AUMC	R	R_adj
0	3.501269 2	1.253125 5	0	0		
0.5	3.615225 6	1.285154 3	1.779123 7	0.451903 2		
1	3.635258 6	1.290680 2	3.591744 7	1.812621		
2	4.285734 8	1.455292	7.552241 4	7.915985 2	-0.626 5752	0.190 1287
4	3.405775 7	1.225472 7	15.24375 2	30.11055 8	0.189 3613	-0.446 2134
6	3.423060 8	1.230535 1	22.07258 8	64.27202 5	0.274 5728	-0.849 2196
8	3.362006 7	1.212538	28.85765 6	111.7064 4		
12	3.429681 8	1.232467 5	42.44103 3	247.8109 1		

Table 17: Calculation Results (Resperidone IV)

Parameter	Unit	Value
Lambda_z	1/h	0.01680329
t1/2	h	41.25068222
Tmax	h	2
Cmax	µg/ml	4.285734848
C0	µg/ml	3.501269235
Clast_obs/Cmax		0.800255241
AUC 0-t	µg/ml*h	42.44103292
AUC 0-inf_obs	µg/ml*h	246.5487852
AUC 0-t/0-inf_obs		0.172140507
AUMC 0-inf_obs	µg/ml*h^2	14843.99606
MRT 0-inf_obs	h	60.20713528
Vz_obs	(mg/kg)/(µg/ml)	0.120690424
Cl_obs	(mg/kg)/(µg/ml)/h	0.002027996
Vss_obs	(mg/kg)/(µg/ml)	0.122099842

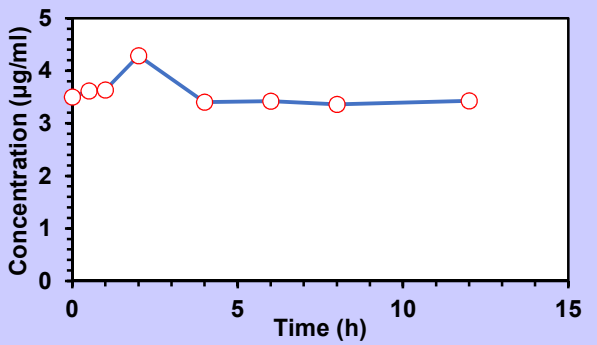

Figure 39: Time in (min) Vs Concentration (µg/ml) [Resperidone IV]

Conclusion:

Non-compartmental analysis showed that Resperidone reached a peak concentration (Cmax) of 4.29 µg/mL at 2 h (Tmax), with a high initial concentration (C0 = 3.50 µg/mL) indicating rapid distribution. The drug exhibited a long half-life (t1/2 ≈ 41.25 h) and mean residence time (MRT0–inf ≈ 60.2 h). Total exposure (AUC0–inf) was 246.55 µg·h/mL, but only 17.2% was captured in the sampling period, indicating most elimination was extrapolated. Observed clearance (Cl_obs) and steady-state volume (Vss_obs) suggest the drug primarily remains in vascular/extracellular compartments.

7. Conclusion

The present study successfully developed a nanosponge-loaded intranasal in situ gel of Risperidone for enhanced brain targeting. The optimized nanosponge formulation (RF1) showed high drug content (96.3%), entrapment efficiency (94.23%), small particle size (152 nm), and good stability, while the optimized in situ gel (MR5) exhibited suitable pH, high viscosity (14,890 cps), strong mucoadhesive strength (1365 dynes/cm²), and

maximum drug content (98.47%). It demonstrated sustained, controlled drug release (98.18%) following zero-order kinetics and remained stable over 3 months. Pharmacokinetic analysis revealed rapid absorption, with Cmax of 4.29 µg/mL (IV) and 3.49 µg/mL (nasal) at 2 h (Tmax) and no absorption lag (Tlag = 0). The drug exhibited a long half-life (t1/2 ≈ 39–41 h) and mean residence time (MRT ≈ 58–60 h), with low volume of distribution (Vss ≈ 0.12–0.14 L/kg), suggesting it largely remains in the vascular compartment. Limited sampling captured less than 21% of total exposure, indicating most of the elimination phase was extrapolated. Overall, the developed intranasal system provides improved nasal retention, controlled release, efficient brain targeting, and prolonged systemic persistence, highlighting its potential for enhanced treatment of CNS disorders with reduced systemic side effects.

Refernces

1. Agrawal M, Saraf S, Saraf S, Dubey SK, Puri A, Patel RJ, Ravichandiran V, Murty US, Alexander A. Recent strategies and advances in the fabrication of nano lipid carriers and their application towards brain targeting. Journal of Controlled Release. 2020 May 10;321:372-415.
2. Béduneau A, Saulnier P, Benoit JP. Active targeting of brain tumors using nanocarriers. Biomaterials. 2007 Nov 1;28(33):4947-67.
3. Goldmann EE. Vitalfärbung am Zentralnervensystem: Beitrag zur Physio-Pathologie des Plexus chorioideus und der Hirnhäute. Königl. Akademie der Wissenschaften; 1913.
4. Pardridge WM. The blood-brain barrier: bottleneck in brain drug development. NeuroRx. 2005 Jan;2(1):3-14.
5. Battaglia L, Panciani PP, Muntoni E, Capucchio MT, Biasibetti E, De Bonis P, Mioletti S, Fontanella M, Swaminathan S. Lipid nanoparticles for intranasal administration: application to nose-to-brain delivery. Expert opinion on drug delivery. 2018 Apr 3;15(4):369-78.
6. Raghav M, Gupta V, Awasthi R, Singh A, Kulkarni GT. Nose-to-brain drug delivery: Challenges and progress towards brain targeting in the treatment of neurological disorders. Journal of Drug Delivery Science and Technology. 2023 Sep 1;86:104756.
7. Li G, Bonamici N, Dey M, Lesniak MS, Balyasnikova IV. Intranasal delivery of stem cell-based therapies for the treatment of brain malignancies. Expert opinion on drug delivery. 2018 Feb 1;15(2):163-72.
8. Li G, Bonamici N, Dey M, Lesniak MS, Balyasnikova IV. Intranasal delivery of stem cell-based therapies for the treatment of brain malignancies. Expert opinion on drug delivery. 2018 Feb 1;15(2):163-72.
9. Geldenhuys WJ, Mohammad AS, Adkins CE, Lockman PR. Molecular determinants of blood–brain barrier permeation. Therapeutic delivery. 2015 Aug 1;6(8):961-71.
10. Miyake MM, Bleier BS. The blood-brain barrier and nasal drug delivery to the central nervous system. American journal of rhinology & allergy. 2015 Mar;29(2):124-7.
11. Ding S, Khan AI, Cai X, Song Y, Lyu Z, Du D, Dutta P, Lin Y. Overcoming blood–brain barrier transport: Advances in nanoparticle-based drug delivery strategies. Materials today. 2020 Jul 1;37:112-25.
12. Agrawal M, Tripathi DK, Saraf S, Saraf S, Antimisiaris SG, Mourtas S, Hammarlund-Udenaes M, Alexander A. Recent advancements in liposomes targeting strategies to cross blood-brain barrier (BBB) for the treatment of Alzheimer's disease. Journal of controlled release. 2017 Aug 28;260:61-77.
13. Pardeshi CV, Belgamwar VS. Direct nose to brain drug delivery via integrated nerve pathways bypassing the blood–brain barrier: an excellent platform for brain targeting. Expert opinion on drug delivery. 2013 Jul 1;10(7):957-72.
14. Singh M, Kumar S, Vinayagam R, Samivel R. Thermosensitive mucoadhesive intranasal in situ gel of risperidone for nose-to-brain targeting: physiochemical and pharmacokinetics study. Pharmaceuticals. 2025 Jun 11;18(6):871.
15. Sipos B, Budai-Szűcs M, Katona G, Csóka I. Gellan gum-based in situ hydrogels for nasal delivery of polymeric micelles loaded with risperidone. Gels. 2025 May 28;11(6):404.
16. Ghazwani M, Vasudevan R, Kandasamy G, Manusri N, Devanandan P, Puvvada RC, Veeramani VP, Paulsamy P, Venkatesan K, Chidmabaram K, Dhurke R. Formulation of intranasal mucoadhesive thermotriggered in situ gel containing mirtazapine as an antidepressant drug. Gels. 2023 Jun 2;9(6):457.
17. Raytthatha N, Shah I, Patel J, Vyas J, Upadhyay U. Development of benzoyl peroxide loaded nanosponges gel. Nat. J. Pharm. Sci. 2021; 1(2):25-9.
18. Swaminathan S, Vavia PR, Trotta F, Torne S. Formulation of betacyclodextrin based nanosponges of itraconazole. Journal of

inclusion phenomena and macrocyclic chemistry. 2007 Apr;57(1):89-94.
19. Adhikari P, Jain SK, Modi S, Nigam V, Shrivas H, Kankane M. Development and In-Vitrocharacterization of risperidone loaded hydroxy propyl beta cyclodextrin nanosponge for enhancing bioavailability.World Journal of Biology Pharmacy and Health Sciences, 2023, 15(03), 139–151.
20. Gaber DA, Alnwiser MA, Alotaibi NL, Almutairi RA, Alsaeed SS, Abdoun SA, Alsubaiyel AM. Design and optimization of ganciclovir solid dispersion for improving its bioavailability. Drug Delivery. 2022 Dec 31;29(1):1836-47.
21. Raja CH, Kumar GK, Anusha K. Fabrication and evaluation of ciprofloxacin loaded nanosponges for sustained release. Int J Res Pharm Nano Sci. 2013;2:1-9.
22. Shah SM, Ullah F, Khan S, Shah SM, de Matas M, Hussain Z, Minhas MU, AbdEl-Salam NM, Assi KH, Isreb M. Smart nanocrystals of artemether: fabrication, characterization, and comparative in vitro and in vivo antimalarial evaluation. Drug design, development and therapy. 2016 Nov 24:3837-50.
23. Sri KV, Santhoshini G, Sankar DR, Niharika K. Formulation and evaluation of rutin loaded nanosponges. Asian J Res Pharmac Sci. 2018 Mar 21;8(1):21-4.
24. Gondokesumo ME, Putra GS, Suhud F, Sulistyowaty MI. In-silico studies and synthesis of 1, 3-benzoxazine derivatives as antimalarial agent through PfATP4 receptor inhibition. International Jurnal Of Pharmaceutical Research. 2021;12(2).
25. Kapadne C, Birari S, Gulecha V, Shinde A, Sambare A, Kshirsagar SK. Formulation and evaluation of budesonide-loaded nanosponges for colon-specific drug delivery systems. BIO Integration. 2024 Jul 1;5(1):979.
26. Yadav DJ, Kunjwani HK, Suryawanshi SS. Formulation and evaluation of thermosensitive in situ gel of salbutamol sulphate for nasal drug delivery system. Int J Pharm Pharm Sci. 2012;4(4):188-94.
27. In vitro and in vivo evaluation of cubosomal in situ nasal gel containing resveratrol for brain targeting
28. Sherafudeen SP, Vasantha PV. Development and evaluation of in situ nasal gel formulations of loratadine. Research in pharmaceutical sciences. 2015 Nov 1;10(6):466-76.
29. Galgatte UC, Kumbhar AB, Chaudhari PD. Development of in situ gel for nasal delivery: design, optimization, in vitro and in vivo evaluation. Drug delivery. 2014 Feb 1;21(1):62-73.
30. Qian S, Wong YC, Zuo Z. Development, characterization and application of in situ gel systems for intranasal delivery of tacrine. International journal of pharmaceutics. 2014 Jul 1;468(1-2):272-82.
31. Fatouh AM, Elshafeey AH, Abdelbary A. Agomelatine-based in situ gels for brain targeting via the nasal route: Statistical optimization, in vitro, and in vivo evaluation. Drug Delivery. 2017 Jan 1;24(1):1077-85.
32. Srivastava RI, Srivastava SA, Singh SP. Thermoreversible in-situ nasal gel formulations and their pharmaceutical evaluation for the treatment of allergic rhinitis containing extracts of moringa olifera and embelia ribes. Int J Appl Pharm. 2017 Nov;9(6):16.
33. Jagdale S, Shewale N, Kuchekar BS. Optimization of thermoreversible in situ nasal gel of timolol maleate. Scientifica. 2016;2016(1):6401267.
34. Shelke S, Shahi S, Jalalpure S, Dhamecha D, Shengule S. Formulation and evaluation of thermoreversible mucoadhesive in-situ gel for intranasal delivery of naratriptan hydrochloride. Journal of drug delivery science and technology. 2015 Oct 1;29:238-44.
35. Jabir SA, Rajab NA. Preparation, in-vitro, ex-vivo, and pharmacokinetic study of lasmiditan as intranasal nanoemulsion-based in situ gel. Pharmaceutical Nanotechnology. 2025 Feb;13(1):239-53.
36. Saudagar RB, Deore SB, Gondkar SB. Formulation development and evaluation of in-situ the nasal gel of lisinoprildihydrate. Sch. Acad. J. Pharm. 2016;5(7):277-83.